Ab initio calculations of thermomechanical properties and electronic structure of vitreloy Zr_{41.2}Ti_{13.8}Cu_{12.5}Ni_{10}Be_{22.5}

Batu Hunca, Chamila Dharmawardhana, Ridwan Sakidja, and Wai-Yim Ching

Phys. Rev. B **94**, 144207 — Published 17 October 2016

DOI: 10.1103/PhysRevB.94.144207

Ab initio calculation of thermo-mechanical properties and electronic structure of vitreloy ($Zr_{41.2}Ti_{13.8}Cu_{12.5}Ni_{10}Be_{22.5}$)

Batu Hunca[1], Chamila Dharmawardhana[2], Ridwan Sakidja[3], Wai-Yim Ching[2]

[1]Trakya University, Physics Department, Faculty of Arts and Science, 22030 Edirne, Turkey

[2]Department of Physics and Astronomy, University of Missouri – Kansas City, Kansas City, MO 64110, USA

[3]Department of Physics, Astronomy and Materials Science, Missouri State University, Springfield, MO 68567, USA

Abstract

The thermo-mechanical properties and electronic structure of vitreloy ($Zr_{41.2}Ti_{13.8}Cu_{12.5}Ni_{10}Be_{22.5}$) are investigated using accurate *ab initio* molecular dynamic (AIMD) simulations and *ab initio* calculations. The structure of the model with 512 atoms is validated by comparison to the experimental data with calculated thermo mechanical properties in good agreement with the exisitng measurements. Detailed calculation of the electronic structure and bonding at the density functional level is obtained for the first time. It is revealed that the traditional definition of bond length in metallic glasses has a limited interpretation, and any theory based on geometrical consideration of the their values for discussion on the structural units in metallic glasses has similarly limited applications . On the other hand, we advocate the use of quantum mechanical based metric, the total bond order desity (TBOD) and their partial compoents or PBOD as valauble parameters to characterise the interatomic bonding in multi-component glasses such as vitrloy.

PACS NO: 71.15.Pd, 81.05.Kf, 74.20.Pq, 62.20.dj

Keywords: Vitreloy, Bulk Metallic Glass, AIMD, Electronic Structure, mechanical properties

1. Introduction

Metallic glass (MG) is a unique class of amorphous materials with some outstanding properties [1-3] compared to conventional metallic alloys and exist in a wide variety of compositions. This is attributed to the absence long-range order (LRO) and grain boundaries, and the presence of the so-called "free volumes" in MGs. Atoms in MGs exhibit strong short-range order (SRO) and medium-range order (MRO) between atoms within their local environment [4-7] which results in their complex yet unique atomic-scale structure. MG was first discovered by Duwez in 1960 [8,9] by rapid quenching of metallic melts of $Au_{75}Si_{25}$ with critical cooling rates of 10^5-$10^6 Ks^{-1}$. However, rapid quenching of the melts with very high cooling rates limits the sample thickness to be thin ribbons for MGs in the early days. There has been many concerted efforts to improve the processing technology and in search for better glass forming alloys with lower critical cooling rates. These efforts motivated researchers to search for amorphous alloys that show high resistance to crystallization from the undercooled liquid state in bulk form. The first bulk metallic glass (BMG) was a Pd-based alloy prepared by Chen using simple suction casting [10]. Since then, the critical cooling rates were significantly lowered [11]. The process has been extended to a wide variety of multicomponent BMGs [12-15] with the Pd-based composites capable of casting in bulk form with cooling rates of less than 10 Ks^{-1}. BMGs have outstanding physical and mechanical properties such as high viscosity, corrosion resistance, high yield strength and hardness, high elastic strain limit etc. Ideal BMG for structural applications should have both excellent glass forming ability (GFA) that avoids crystallization and intrinsic ductility that minimizes brittle fracture [16]. When metals with significantly different atomic radii are alloyed in certain percentages, the inclination to crystallize is greatly hindered. Thus it is imperative to understand both SRO and MRO, which determine the packing of atoms. This can only be achieved by realistic large scale modeling and rigorous first-principles calculations of electronic structure and bonding in BMGs. This is considered to be one of the Holy Grails in understanding the fundamental issues in non-crystalline solids in general and in BMG specifically [17-20].

One of the most intriguing multicomponent BMGs is vitreloy such as $Zr_{41.2}Ti_{13.8}Cu_{12.5}Ni_{10}Be_{22.5}$ (Also known as Vit1) first introduced by Peker and Johnson in 1993 [21]. Vitreloy usually have more than 5 different atomic species of vastly different atomic sizes and a wide range of composition ratios. For instance, the atomic radius of Zr is 84% larger than Be. The exact structure of Vit-1 at the atomic scale however is not known and accordingly, theoretical calculation on its electronic properties is still non-existent.

Vit-1 alloys exhibit an extraordinary high glass forming ability (GFA) with a low critical cooling rate (1 Ks^{-1}) [21] and superior mechanical properties [22,23]. There have been a large body of experimental works done on Vit-1 to characterize and optimize several key materials parameters [24-33]. Vit-1 has a glass transition temperature (T_g) of 623 K [24], an onset temperature of crystallization (T_x) of 705.0 K, a melting temperature (T_m) of 933.0 K, a mass density of 6.11 $g.cm^{-3}$ and a GFA parameter of 0.67 as defined by the ratio of the glass transition to the liquid temperature (T_g/T_l). Other relevant work include analyses on the thermodynamics properties [25], chemical inhomogeneity[26], self-diffusion [27], viscosity [28], primary crystallization [29], internal structure [30] and mechanical properties [24,31-33]. Busch et al used the differential scanning calorimetry (DSC) measurement to investigate the thermodynamic properties [25] and to assess the difference in Gibbs free energy between the thermodynamically stable crystalline phases and the undercooled melt. The high GFA of Vitreloy has been attributed to a very small difference in the free energy between the liquid and the solid state unlike those observed in other metallic glasses. The chemical and structural homogeneity of Vit-1 were investigated by atom probe field ion microscopy and transmission electron microscopy (TEM) [26], showing phase separation in the undercooled liquid state and a significant composition fluctuations for Be and Zr but not in the Ti,Cu and Ni concentration. The mechanism for self-diffusion of Be in supercooled liquid state in Vit-1 was investigated by Geyer et al [27]. Viscosity was measured in the entire temperature range from the melting point to the glass transition temperature [28]. Primary crystallization and decomposition in this structure were studied by small angle neutron scanning (SANS), TEM and DSC [29]. Gerold and co-workers investigated the local atomic correlations in Vit-1 using wide angle neutron scattering experiments to obtain the structure factors [30]. Fracture toughness was measured by Conner et al [31], and Gilbert et al [32]. The

flow behavior of the supercooled liquid was studied by Waniuk [33] in isothermal three-point beam-bending experiments. The uniaxial stress-strain behavior of Vit-1 over a wide range of strain rates and temperatures was reported by Lu [24].

On the simulation front, there has been the finite element modeling to understand the non-isothermal channel flow of Vit-1 and to elucidate the transition to non-Newtonian flow and shear localization by contrasting the computed flow evolution onto an experimentally developed flow diagram [34]. Time-temperature-transformation curve for Vit-1 has also been studied to address the primary factors influencing their GFA [35]. At the atomic scale however, the only work we are aware of is the atomistic calculations in terms of structure factors, pair correlation functions, coordinate numbers, bond pairs and Voronoi polyhedra analysis using *ab-initio* molecular dynamics (AIMD) by Hui et al [36] on a relatively small model of 200 atoms. Hui [36] was able to identify apparent geometric characteristics of the SRO's network and discussed the possible occurrence of an icosohedral MRO that constructed from these icosahedral SRO's as a key stabilizing factor for Vit-1. These types of structural stability analyses however were based on geometric considerations. So far, critical information and understanding on the electronic properties and atomic-scale interactions in relation to the SRO and MRO of the Vit-1 are still missing. Thus, there is an urgent need to investigate the underlying role of the internal chemical bonds on the stability and overall mechanical properties of a complex BMG's such as Vit-1.

Indeed, the main difficulties for electronic structure calculation of BMG has been the lack of realistic and sufficiently large structural models in the form of supercells and reliable method for electronic structure calculation. Classical molecular dynamics (MD) which rely on well calibrated potential functions have been the main simulation tool used for binary or ternary BMGs [36-43]. For multicomponent BMG, the development of such potentials is extremely difficult if not impossible and the only way to unravel the correct structures based on which electronic structure calculations can be performed is to use *ab initio* molecular dynamics (AIMD) using density functional theory (DFT). The computational resources required would be orders of magnitude more than classical MD and as a results, most AIMD simulations are restricted typically to relatively small size models [36,44-46].

In this work, we report the results on the calculation of the thermo-mechanical properties and the electronic structure of Vit-1 using AIMD on a sufficiently large model of 512 atoms. The orthogonalized linear combination of atomic orbitals (OLCAO) method [47]is used to calculate the electronic structure and interatomic bonding. In the following section, we outline the computational procedures adopted and the methods used. The results obtained are presented and discussed in section 3. A brief summary with main conclusions are given in the last Section 4.

2. Methodology

2.1 Model construction

Our strategy to simulate the Vit-1 alloy starts with randomly placing 512 atoms (211 Zr, 71 Ti, 64 Cu, 51 Ni and 115 Be.) with a composition close to $Zr_{41.2}Ti_{13.8}Cu_{12.5}Ni_{10}Be_{22.5}$ in a periodic cubic supercell with a size of 2.0292 x 2.0292 x 2.0292 nm^3 consistent with its mass density. Next, this random model is subjected to simulated annealing and optimization using Vienna *Ab initio* Simulation Package (VASP) [48-50]. We use AIMD at constant pressure and temperature (NPT) ensemble with the following specifications: (1) The PAW-PBE potentials [51] within the generalized gradient approximation(GGA) [52]; (2) electronic convergence criterion set at 10^{-4}eV with an energy cutoff of 400 eV; (3) time-step of 3 fs; (4) a single Γ point sampling. We have tested the AIMD simulations at a higher energy cutoff, but no significant improvement was observed. For temperature and pressure we use Langevin thermostat that is implemented in VASP 5.3 for the NPT simulations. The appropriate friction coefficients for the thermostat [53]were chosen so as to optimize the ionic convergence and total simulation time. Details on the selection process has been given elsewhere in our previous *ab-initio* MD publications [54,55].

Hui et al [36], had used the AIMD in VASP back in 2009 with NVT for the annealing process available at that time on a smaller cell of only 200 atoms for vitroloy. We used the NPT ensemble which is more suitable since volume changes during annealing and alloying, [54]. The AIMD works in two stages. We first melt the 512-atom model at temperatures above the melting temperature (932K). Second, the melted model was quenched sequentially from 1500K to 300K in 8 satges with an average cooling rate of 6 x 10^{13} Ks^{-1}. At each stage of quenching, the model was held at respective temperatures for 600 time-steps with 2 fs per unit time step. At each stage of cooling the thermodynamic fluctuations were closely monitored to ensure realistic quenching.

After final relaxation at 300 K, we select snapshots from the 600 steps of MD run that are closest to 300 K. The selected models were then fully relaxed at constant volume and the structure was chosen as the most appropriate model from the quenching process. The calculated densities (6.055 g cm^{-3}) of the final models were slightly lower, but in good agreement with the experimental density of 6.11 g/cm^3, at 300K [31]. The lower density can be simply understood from the fact that our quenching rate for the AIMD simulations is much higher than that from experiments, yielding a larger glass volume. Nethertheless, this procedure provides the most representative structure at the given temperature [55]. We emphasize that this filtering process we implemented is crucial to obtain reliable structure. Three glass models were obtained using the procedures described and their final structural parameters are listed in **Table 1**. A snapshot of the final configuration is shown in **Fig. 1.** Since Model 2 has the lowest total energy, it is chosen for the subsequent calculation of the electronic structure.

Table 1. Cell parameters for the 3 models.

	a (Å)	b (Å)	c (Å)	α (^{0})	β (^{0})	γ (^{0})
Model 1	18.5544	20.9830	21.9667	95.6	88.7	82.4
Model 2*	18.5633	19.8353	23.1185	87.6	95.00	84.3
Model 3	18.5619	19.8354	23.1161	87.6	95.00	84.3

2.2 Properties calculation

2.2.1. Thermo-mechanical properties:

The VASP relaxed crystal structures are used to calculate the 2nd order elastic tensors for the three Vit-1 models using an efficient stress-strain method [56] to obtain bulk modulus (K), shear modulus (G), Young's modulus (E) and Poisson's ratio γ. These are important structural parameters to understand the fracture toughness of Vitreloy [31],[32]. A strain of +0.5% and -0.5% is applied to the cell to obtain the stress data σ_j. From the calculated σ_i data (i, j = 1, 2, 3, 4, 5, 6), the elastic coefficients C_{ij} are evaluated by solving the linear equation $\sigma_i = \sum_{j=1}^{6} C_{ij}\varepsilon_j$. The averaged mechanical properties: K (bulk modulus), G (shear modulus), E (Young's modulus), and γ (Poisson's ratio) are then obtained based upon the Voigt–Reuss–Hill (VRH) approximation

for polycrystals. The Voigt approximation [57] assumes a uniform strain in the structure and gives the upper limit for the mechanical properties derived from the elastic coefficients C_{ij} whereas the Reuss approximation [58] assume a uniform stress distribution which gives the lower limit through the elastic compliance tensor S_{ij}. The average of these two limits is known as Hill approximation [59] and is usually taken as a reasonable representation of the calculated mechanical properties of a material.

2.2.2. Electronic structure

The electronic structure and bonding of the vasp-relaxed model for Vit-1 are calculated using the all electron orthogonalized linear combination of atomic orbitals (OLCAO) method [60],[47]. The OLCAO method is a first-principles DFT-based method using atomic orbitals as the basis and it is very efficient and flexible for materials with complex structures such as multi-component BMGs. Atomic orbitals are used in the basis expansion where the radial part is expanded in the terms of Gaussian-type of orbitals (GTOs). The solution of Kohn-Sham equation in the OLCAO method provides the energy eigenvalues and wave function from which the density of states (DOS) and other physical properties can be evaluated. Effective charges on each atom (Q^*) and bond order (BO) values between every pair of atoms can be obtained using the Mulliken scheme [61]. The Q^* and BO are given by:

$$Q_\alpha^* = \sum_i \sum_{n,occ} \sum_{j,\beta} C_{i\alpha}^{*n} C_{j\beta}^n S_{i\alpha,j\beta} \quad (1)$$

$$\rho_{\alpha\beta} = \sum_{n,occ} \sum_{i,j} C_{i\alpha}^{*n} C_{j\beta}^n S_{i\alpha,j\beta} \quad (2)$$

Where $C_{i\alpha}^{*n}$ is the eigenvector of the n^{th} band state and $S_{i\alpha,j\beta}$ is the overlap matrix between atoms; α and β represent atoms whereas i and j designate the orbitals in the atoms.

The sum of all BO pairs gives the total bond order (TBO). When divided by the volume of the cell, we obtain the total bond order density (TBOD) which is an important quantum mechanical metric to characterize the strength of the materials such as BMGs. Although BO generally related to the distances of separation of the atomic pairs, it also depends on local atomic arrangements of that pair of atoms which is especially important for BMGs. TBOD is much more

useful than geometric parameters such as atomic radii, atomic size, bond length, and cut-off distances etc. which cannot be precisely defined in BMG. In fact, the BO is a single well-defined descriptor irrespective of the nature of the bonding, be it ionic, covalent, metallic, H-bonding, or non-directional bonding as in BMGs. The use of BO and TBOD in different materials systems has been demonstrated in several recent publications [62-72].

3. Results and Discussion

3.1 Structure and topology of Vit-1 models

The total pair distribution function (PDF) G(r) of our model for $Zr_{41.2}Ti_{13.8}C_{12.5}Ni_{10}Be_{22.5}$ is shown in **Figure 2(a)**. A normalizing coefficient was used to align with the experimental data in the Y-axis. The very good agreement with the experimental PDF [30] validates our model. In a multicomponent BMG, it is a great experimental challenge to resolve the total RDF into partial components, or the PRDF. This is particularly a daunting task for Vit-1 with five different components. On the other hand, this information is readily available from the modeled structure. **Figure 2(b)** shows the contributions to the total PRDF from 8 most dominant pairs in the Vit-1. The experimental observation of the first prominent peak at 2.3 Å actually consists of contributions from Be-Be, Ni-Be and Cu-Be pairs. The main broad peak centered at 2.75 Å consists of contributions from many pairs (Zr-Be, Zr-Cu, Zr-Ni and Zr-Ti) but the details are all buried in the superposition. Our PRDF indicates that the predominating contribution to this main peak comes form Zr-Be and Zr-Cu pairs whereas the slight shoulder around 2.98 Å is from Zr-Zr pairs mediated by the Zr-Ti pair in between. It appears that the Zr-Ti pairs at 2.98 Å tend to overestimate the PDF compared to experimental data (see insect of **Fig. 2(a)**). It is clearly seen that the first shell, defined as the distance for the first deep minimum (3.7 Å) in the measured PDF is densely packed in this multi-component amorphous glass. The peak positions for the PRDF in the first shell are listed in **Table 2**, and compared to experimental estimations [28] and Hui's studies [36] using a smaller sized model.

Table 2. Peak positions for the pairs in the first shell of the PDF plot.

	Be-Be	Ni-Be	Cu-Be	Zr-Ni	Zr-Cu	Zr-Be	Zr-Ti	Zr-Zr

Experimental [30]	2.23	2.33	2.39	2.74	2.83	2.87	3.04	3.19
Hui [36]	2.19	2.28	2.29	2.68	2.82	2.73	2.98	3.15
Present work	2.19	2.27	2.29	2.67	2.76	2.75	2.98	3.16

3.2 Thermal-mechanical properties

Glass transition temperature T_g is an important parameter to characterize the effectiveness of glass formation. We can obtain T_g from AIMD. In **Figure 3** the internal energy as a function of temperature is plotted and data are linearly fitted to temperature ranges between 1500 to 700 K and 600 to 300 K. The intersection point of these two straight lines [31] gives T_g of 635 K, very close to the experimental value is 623 K [24] obtained from DSC measurement when subjected to a cooling rate of 20 K/min. This value is also consistent other simulation studies as well [36,73]. The close agreement of simulated *Tg* with experiment again validates our annealing protocol adopted in this study and that the final model we obtained for Vit-1.

Thermal expansion of crystals is mainly caused by the anharmonicity of atomic vibrations. For BMG, the noncrystalline disorder at atomic scale provides extra complications to the themal expansion which are related to specifc disorder such as the presence of free volume, vacancy keinetics, glass transition temperature and glass forming ability, and unclear information about the nature of interatomic bonding [74]. Thus calculation of the coefficent of thermal expansion (CTE) in BMG via AIMD direct method [55] can provide important insight about BMG system. However the fulctuation of thermal properties in AIMD simulation must be carefully monitored in order to accurately evaluate the CTE. **Figure 4(a)** shows the volume fluctuation at each temperature during the simulated annealing process. Here after each annealing step the temperature was held at constant (See Methods Section 2) so the cell has enough time to equilibrate. **Figure 4(b)** shows the plot of average volume as a function of temperature from 300K to 2400K. The smooth variation indicates the fluctuation is fairly small and within an acceptable limit. The isotropic CTE can be estimated by using the formula [55]

$$\alpha_V = \frac{1}{V_0}\frac{dV}{dT} \tag{3}$$

where, V_0 is the equilibrium volume at room temperature (300 K). We fit the data in **Figure 4 (a**) to a 2^{nd} order polynomial a formula of V_T (normalized to 512 atoms) = 8406.34 + 0.27 x T + 6.16 x 10^{-5}x T^2 $Å^3$. The goodness of the fit (R-Square is 0.99981) enables us to determine CTE at 298K to be 3.61 x 10^{-5} K^{-1} which is close to the measure value of 4.0 x 10^{-5} K^{-1} [73]. Recent studies by Jiang et al [74] also confirms that as-cast Vit-1 shows a gradual decrease in CTE with the decrease of temperature. They show that the thermal expansion is different from the furthered annealed Vit-1 and crystalline Vit-1and from as-cast Vit-1 (obtained from vendor). Annealed Vit-1 shows a sudden jump in CTE and crystalline shows a constant CTE from melt.

3.3 Bulk mechanical and elastic properties

BMGs show a remarkable high strength and high elastic strain limit compared with the crystalline alloys. On the other hand, relaxation-induced embrittlement can occur mostly related to the presence of free volume that affect its plasticity. Poisson's ratio (ν) and Pugh modulus ratio G/K are some of the key parameters to gauge its toughness. Shear modules G and bulk modulus K represent the resistance to shear flow and resistance to volume dilatation of a materials whereas Young's modulus E accounts for the contraction in the direction perpendicular to dilation. We present the mechanical parameters derived from calculated elastic coefficient (See Method section) for Vit-1 in **Table 3**. The calculated values of K, G, E and Poisson's ratio ν slightly underestimate the experimental data [22,23,75]. This underestimation can be understood from the fact that our simulated glass has a slighly lower weight density or a relatively larger molar volume. It has been shown from experimental works in Zr-based BMG's [76-78] that the Zr-based BMG with a larger molar volume, normally procured from a faster quenching rate from the melt, would result in relatively lower elastic properties. Nevertheless, this is well within the expected range for calculations using a stress-strain approach. A good measure for toughness is Pugh modulus ratio G/K. A low Pugh's modulus ratio typically favors ductility [68,79-81]. Our model for Vit-1shows it to be a slightly more ductile BMG than those reported by Lewandoski [75] and Johnson [23]. Since our model has a relatively lower density, a higher molar volume due to the high cooling rate used to quench the simulated melt, this is quite consistent with that experimental findings that have demonstrated that the higher the cooling rate, the more compressive plasticity that Zr-based BMG exhibits[76]. In addition, Table 3 shows the

approximately isotropic nature of the elastic constants, which is typical for noncrystalline glasses. This also further validates our modeling approach to use a large number of atoms (512) which is essential to ensure a better estimate of their elastic properties.

Table 3. Mechanical properties and elastic constants of $Zr_{41.2}Ti_{13.8}Cu_{12.5}Ni_{10}Be_{22.5}$

	K (Gpa)	*G (Gpa*	*E (Gpa)*	*ν*	*G/K*
Lewandowski [75]	114.7	37.4	101.3	0.341	0.324
Johnson [23]	111.2 114.1	35.9 34.1	97.2 95.0	0.354 0.352	0.369
Calculated (Hill)	108.2	29.1	80.2	0.376	0.269
Calculated (Voigt)	108.2	29.2	80.3	0.376	0.270
Calculated (Russ)	108.1	29.1	80.0	0.377	0.269
Elastic stiffness constants					
C_{11}	146.8	C_{44}	28.8	C_{12}	88.3
C_{22}	148.3	C_{55}	29.1	C_{13}	88.2
C_{33}	146.5	C_{66}	29.4	C_{23}	89.4

3.4 Electronic structure and bonding

As mentioned in the introduction, accurate electronic structure calculations using *ab initio* methods on large models of BMG are very expensive and rarely done. It is non-existent for Vit-1. Using the versatile OLCAO method, we are able to obtain detailed information on the electronic structure and interatomic bonding in Vit-1 based on the 512 atom supercell model constructed using AIMD. **Figure** shows calculated total density of states (TDOS) and its decompositions into PDOS of 5 different component atoms in the range of -10 eV to 10 eV (The Fermi level is set the 0.0 eV). The main feature of TDOS is a slanting plateau from high end at -4 eV to lower end at 4 eV. The highest value of DOS at –4.0 eV originates from the more localized contribution of Cu-3d states. The main interest is the states at or near the Fermi level E_F since it has been proposed that the existence of a local minimum in the TDOS at the Fermi level or $N(E_F)$ is a contributing factor of the stability of metallic alloys [82]. On the first look, it appears

that E_F does locate in the vicinity of a local minimum in the TDOS that appears to verify that the stability of vitreloy at this composition. However, such a conclusion is clearly premature at best for the following reasons. (1) The minimum is not prominent since there are many other local minima and maxima not too far from E_F and the question is how close to the E_F should the local minimum be defined. This is an important question that has seldom been scrutinized. (2) The calculation is based on a three models with 512 atoms in the supercell. Even though this is the largest *ab initio* calculation that has been done, the result could easily depend on the size of the model and sampling of the distributions of its constituent atoms. (3) No rigorous theory actually exists that can attribute the stability of BMG purely on a single parameter $N(E_F)$ which could depend on may other factors related to the kinetics such as the cooling rate and change in the interatomic bonding during the quenching process other than the mere composition. Nevertheless, the value of $N(E_F)$ and its composition is important for other properties such as electric conductivity and transport properties in metallic systems. Our calculated value of 468.7 states per unit cell per volume (or 0.916 states per atom per eV) for $N(E_F)$ is fairly large for a metallic alloy. In **Table 4**, we list the contributions to $N(E_F)$ from the 5 atomic species. The largest contribution is from Zr followed by Ti since E_F are derived mostly from the Zr-4d and Ti-3d orbitals and they also have large atomic percentage. Although Be has 22.5% atomic percentage in Vit-1, it has minimal contribution of only 7.44% to $N(E_F)$ since it does not have any occupied *d* electrons. Both Cu and Ni have they *3d* orbitals but these states are well below the Femi level.

Table 4. Energy values and contribution percentages for each component at the Fermi Level.

	Zr	**Ti**	**Cu**	**Ni**	**Be**	**Total**
PDOS State [eV Cell]	250.969	106.455	33.9444	42.519	34.8595	468.748
Contribution % to TDOS	53.54	22.71	7.24	9.07	7.44	100

Information on the interatomic bonding is extremely important for all materials but especially so for BMGs. Unlike the covalent or ionic bonding in inorganic materials, the interatomic bonding in BMG is ill-defined because of the lack of specific definition of the "bond length" (BL) and the influence of all nearby atoms around the target atom as part of the multi-atomic metallic bonding. This impediment is further exuberated by the long standing notion of "free volume" which is difficult to define in luau of the metallic nature of the bonding characters within the BMG's. We have calculated the bond order values (BO) for all pairs of atoms in the model up to 5 Å distance

of separation for the pairs (for simplicity, we call this distance of separation instead of "BL" with the understanding that this BL cannot be defined in the usual sense for BMG). The plot of BO vs BL is shown in **Figure 6(a)-(c)**. There are 15 different possible pairs and for clarity, we divide the plot into three parts. **Figure 6(a)** shows the plot for 5 Zr-related pairs and **Figure 6(b)** for the 4 Be related pairs since Zr (Be) is the largest (smallest) of the 5 types of atoms. **Figure 6(c)** shows the plot for the other 6 pairs (Cu-Cu, Ni-Ni, Ti-Ti, Cu-Ni, Ti-Cu, and Ti-Ni). These are very busy figures and the main observations can be summarized as follows: (1) Although, the general trend in this scattered plots of BO vs. BL is in a decreasing order, it is important to note that for a give pair of atoms with a fixed BL, there is wide range of values for the BO, and for a fixed BO value the BL can span fairly large distance of separation, accentuating the assertion that the BL in BMG is an ill-defined quantity. The vertical dashed line at 3.7 Å is the first minimum in the PDF generally used to define the boundary of the first shell of atoms in glasses. (2) The highest BO comes from Be-Be pairs with short range of separation showing the unique role played by small Be atoms in the formation of vitreloy. (3) Other than Be-Be, Cu-Be and Ti-Ti pairs also have strong bonding with BO values up to 0.290, 0.250 and 0.284 respectively. Thus Ti also plays a key role in the Vit-1 structure by forming strong bonds with other components even though its percentage is not large. (4) Zr-Cu and Zr-Be bond orders are the smallest amongst other pairs mainly due to the large size of Zr atoms resulting in larger distance of separation. (5) Ni-Be pairs have the small bond length resulting in high BO values. (6) Generally speaking, the BO values diminish quickly beyond 3.7 Å, the first minimum in the RDF of **Figure 2(a)**, some of them come from the second "nearest neighbor" atoms but they are not negligible and can make significant contributions to the TBOD (see discussion below). (7) The scattered plot of BO vs BL collaborates well with the RDF of **Figure 2(b)** showing every pair fits well with the experimental [30] PDF. Namely, the first peak consists of Be-Be, Be-Ni and Be-Cu pairs. Second peak consists of Zr-Be, Zr-Ni, Zr-Cu and Zr-Ti pairs and the shoulder around 2.98 Å is caused by the Zr-Zr pairs.

From the BO values for all interatomic pairs, we can obtain the total bond order for that pair of atoms by adding them together and normalize by the volume of the cell, we have the bond order density (BOD). When the BOD of all pairs are added, we have the total BOD (TBOD) which is a single quantum mechanical metric best describe the interatomic cohesion of a crystal or a glass

in the present case [67,69]. The use of TBOD in characterizing different type of materials is a novel concept that we advocate since the volume of the system is part of the metric. For example, it can be used to determine the stability of a BMG with different compositions. In **Figure 6(d)**, we show in the form of a Pie chart the percentage contribution from different pairs to the TBOD in Vit-1. It is seen that Zr-Be and Zr-Zr are the biggest contributors to the TBOD with the largest numbers of atoms and the largest number of partial bond order density (PBOD) with percentage of Zr-Be and Zr-Zr pairs to be 13.65 % and 15.75 % respectively. This chart includes both the effect of the composition and the strength of the bonds into account, a level higher than just using the composition or the size of the atoms.

The significance of the BO-BL's distribution can also be linked to the previous observation on the role of bond pairs on the mechanical properties of a wide range of BMG's as suggested by Ma et al.[22] and observed very recently in the *in-situ* EXAFS study conducted by Antonowics et al.[83]. Ma et. al. [22] reasoned there is a significant role of the solvent-solvent interaction that contributes to the "weakest link" within these BMG which in turn, defines the Young's modulus and shear modulus. They argued that weaker Zr-Zr bond along with the relative segregation of the solvents around the perimeter of the solute-center clusters determines the degree of overall compliance of these BMG's. To support this argument, they compared the values of the enthalpy of mixing of Zr-Zr with those of Zr-X's, where X is the solute constituent. Antonowics et al. [76] just recently reported an *in-situ* EXAFS study on $Zr_{66.7}Cu_{33.3}$ metallic glass under hydrostatic pressure up to 38.6 GPa. They too noted that the softer Zr-Zr bond essentially controls the degree of compressibility of the metallic glass. Furthermore, they were able to observe the large variation in the BL of the more compliant Zr-Zr bonds. The Zr-Zr BL statistics are apparently quite sensitive toward hydrostatic compression such that it can be used to quantify the stress accommodation within the glass. In this regard, we would like to especially point out that our BO-BL data provided in **Figure 6** should be able to furnish a more expansive and quantitative assessment on these essential pair-bond statistics as well as pair-bond dynamics within Vit-1 especially during deformation. One can see, for example, that the expected average BO for Zr-Zr is indeed relatively smaller than those of Zr-X's. As shown in the pie-chart in **Figure 6(d)**, the Zr-Zr pairs do represent one of the largest constituent of BOD within the glass structure. Furthermore, by using our BO-BL data that is coupled with the Cartesian 3D mapping of the

individual pairs within the BMG structure, we would be able to fully assess the degree of contiguity of presumably more compliant Zr-Zr solvent-solvent bonds as well as the dynamics of such bonds during deformation. The previous works [23,84,85] have pointed to the essential presence of a cooperative shear motion of atomic clusters termed shear transformation zones (STZ) shear modulus facilitated by the free volume formation [86,87] to enable an enhanced plasticity in BMG's. While such a pictorial description of a prerequisite to liberate the shear motions is very evident, a concurrent description on the bonding dynamics within internal glass structures during deformation will be also quite useful in the efforts to further improve the overall mechanical properties of the BMG's.

To illustrate further the importance of the Bond Order consideration, we took snapshots of 4 sketches of atomic positions in Vireloy model based on their radial distance with the center atoms in **Figure 7**. Namely, we depict (a) Be centered (with largest Be-Be BO), (b) Be centered (with smaller Be-Be BO). The Be atoms chosen are the ones with Be-Be BL is at a constant bond length of 2.18 Å. In (c), Zr centered (with largest Zr-Zr BO) and (d) Zr centered (with smaller Zr-Zr BO) clusters are represented radially. Note that this is not to imply an average packing of each type of cluster, rather this is solely to show the projected radial sampling of the surrounding atoms within the vicinity of the center atoms based on the existence of the paired bonds. The Zr atoms chosen are the ones with Zr-Zr BL is at 3.07 Å. We would like to point out that despite the similar bond length in (a-b) and (c-d), there is a great deal of heterogeneity with respect to the surrounding neighboring atoms crowding the center atom. Thus, a stability analysis that is solely predicated upon the use BL and connected pairs would certainly lose the role of many-body interactions that contribute the strength of the bonds. The multi-center bonding characteristic inherent in these complex structures certainly would warrant a more comprehensive quantum mechanics approach to both their stability as well as the overall mechanical properties.

Next we present the results of effective charge Q^* in Vit-1 according to Eq. (1). They are shown in **Figure 8** with the average values indicated. Also shown are the distribution plots in the form of histogram. It can be seen that the average Q^* values for the atom types are 3.46 e^- for Zr, 3.87 e^- for Ti, 11.74 e^- for Cu, 10.39 e^- for Ni and 2.49 e^- for Be. The valence shell electrons in a

neutral atom for these atoms are: Zr (4), Ti (4), Cu (11), Ni (10) and Be (2). So on average Zr and Ti lose 0.54 e^- and 0.13 e^- electrons respectively whereas Cu, Ni and Be gain electrons in the amount of 0.74 e^-, 0.39 e^- and 0.49 e^- respectively. The histogram distribution of the effective charges for each type of atom is shown on the right panel in **Figure 8** which shows a reasonable range in the form of Gaussian distribution except Ti which has a wider range of Q*. However, there can be atoms of the atomic type which can lose or gain electrons different from their average values. This is completely different from the case of inorganic glasses where specific type of atoms either gain electrons or lose electrons from their neutral state. The difference in the charge transfer may have a profound implication toward the degree of ductility within the BMG. For instance, Rouxel and Y. Yokoyama [88] have recently demonstrated that the ductility in metallic glass can be closely linked to a small net charge transfer and a weak-bond directionality. Our results suggested that our glass model does exhibit these characteristics. Furthermore, a complete mapping of the net effective charge as shown in **Figure 8** will certainly be needed to search for relatively ductile BMG's. This fact further demonstrates the complex nature of interatomic bonding in metallic glasses, especially in multi-component BMG's such as Vitreloy.

4. Conclusions

We have successfully constructed a reasonably large model for vitreloy ($Zr_{41.2}Ti_{13.8}Cu_{12.5}Ni_{10}Be_{22.5}$) using accurate *ab initio* MD simulations. The structure of the model is validated by comparison to the experimental data especially in the detailed analysis of pair distribution function. Our calculations results on the thermo mechanical properties of this model are in good agreement with the exisitng measurements further strengthening the credibilty of the model. Detailed calculation of the electronic structure and bonding in vitreloy at the density functional level is especially significant since no such results are available. The lack of such information in the literiture is attributed to the lack of accurate structural models of reasonable size and sutable methods for the electronic structure calculation. The most important revealation is the fact that the traditional definition of bond length in metallic glasses has no valid meaning, and any theory based on geomtrical consideration of the their values for discussion on the structural units or short range and intermediate range orders becomes questionable. On the other hand, we advocate the use of quantum mechanical based metris, the total bond order desity (TBOD) and their partial compoents or PBOD as valauble parameters to characterise the interatomic bonding in multi-

component glasses such as vitreloy. For future work, we would like to use larger models for more accurate results and to investigate the effect of variations in compositons for vitreloy such that the procedures and methods used can be more predictive in searching for BMGs with superior properties. This would require adequate computational resources but is not an unsummotable obstacle.

Acknowledgements

This research used the resources of the National Energy Research Scientific Computing Center supported by DOE under Contract No. DE-AC03-76SF00098.

REFERENCES

[1] A. L. Greer, Science **267**, 1947 (1995).
[2] M. Ashby and A. Greer, Scripta Materialia **54**, 321 (2006).
[3] A. L. Greer, Materials Today **12**, 14 (2009).
[4] W. Luo, H. Sheng, F. Alamgir, J. Bai, J. He, and E. Ma, Physical review letters **92**, 145502 (2004).
[5] D. B. Miracle, Nature materials **3**, 697 (2004).
[6] H. Sheng, W. Luo, F. Alamgir, J. Bai, and E. Ma, Nature **439**, 419 (2006).
[7] Y. Shi and M. Falk, Scripta materialia **54**, 381 (2006).
[8] P. Duwez, R. Willens, and W. Klement Jr, Journal of applied physics **31**, 1136 (1960).
[9] W. Klement and R. Willens, (1960).
[10] H. Chen, Acta Metallurgica **22**, 1505 (1974).
[11] H. Kui, A. L. Greer, and D. Turnbull, Applied Physics Letters **45**, 615 (1984).
[12] A. Inoue, Materials Science and Engineering: A **304**, 1 (2001).
[13] W.-H. Wang, C. Dong, and C. Shek, Materials Science and Engineering: R: Reports **44**, 45 (2004).
[14] J. Schroers, Physics Today **66**, 32 (2013).
[15] J. F. Löffler, Intermetallics **11**, 529 (2003).
[16] W. Wang, Advanced materials **21**, 4524 (2009).
[17] J. C. Mauro, A. Tandia, K. D. Vargheese, Y. Z. Mauro, and M. M. Smedskjaer, Chemistry of Materials **28**, 4267 (2016).
[18] K. J. Laws, D. B. Miracle, and M. Ferry, Nat Commun **6** (2015).
[19] J. L. Finney, Nature **266**, 309 (1977).
[20] D. B. Miracle, Nat Mater **3**, 697 (2004).
[21] A. Peker and W. L. Johnson, Applied Physics Letters **63**, 2342 (1993).
[22] D. Ma, A. D. Stoica, X. L. Wang, Z. P. Lu, B. Clausen, and D. W. Brown, Physical Review Letters **108**, 085501 (2012).

[23] W. L. Johnson and K. Samwer, Physical Review Letters **95**, 195501 (2005).
[24] J. Lu, G. Ravichandran, and W. L. Johnson, Acta materialia **51**, 3429 (2003).
[25] R. Busch, Y. Kim, and W. Johnson, Journal of applied physics **77**, 4039 (1995).
[26] R. Busch, S. Schneider, A. Peker, and W. Johnson, Applied physics letters **67**, 1544 (1995).
[27] U. Geyer, S. Schneider, W. Johnson, Y. Qiu, T. Tombrello, and M.-P. Macht, Physical review letters **75**, 2364 (1995).
[28] R. Busch, A. Masuhr, E. Bakke, and W. L. Johnson, in *MRS Proceedings* (Cambridge Univ Press, 1996), p. 369.
[29] S. Schneider, P. Thiyagarajan, and W. Johnson, Applied physics letters **68**, 493 (1996).
[30] U. Gerold, A. Wiedenmann, R. Bellissent, M.-P. Macht, and H. Wollenberger, Nanostructured Materials **12**, 605 (1999).
[31] R. D. Conner, A. J. Rosakis, W. L. Johnson, and D. M. Owen, Scripta Materialia **37**, 1373 (1997).
[32] C. Gilbert, R. Ritchie, and W. Johnson, Applied Physics Letters **71**, 476 (1997).
[33] T. Waniuk, R. Busch, A. Masuhr, and W. Johnson, Acta materialia **46**, 5229 (1998).
[34] M. D. Demetriou and W. L. Johnson, Acta Materialia **52**, 3403 (2004).
[35] S. Mukherjee, J. Schroers, W. Johnson, and W.-K. Rhim, Physical review letters **94**, 245501 (2005).
[36] X. Hui, H. Fang, G. Chen, S. Shang, Y. Wang, J. Qin, and Z. Liu, Acta Materialia **57**, 376 (2009).
[37] G. A. Almyras, D. G. Papageorgiou, C. E. Lekka, N. Mattern, J. Eckert, and G. A. Evangelakis, Intermetallics **19**, 657 (2011).
[38] Y. Q. Cheng and E. Ma, Progress in Materials Science **56**, 379 (2011).
[39] M. F. de Oliveira, G. A. Almyras, and G. A. Evangelakis, Computational Materials Science **104**, 92 (2015).
[40] K.-H. Kang, K.-W. Park, J.-C. Lee, E. Fleury, and B.-J. Lee, Acta Materialia **59**, 805 (2011).
[41] C. Tang and C. H. Wong, Intermetallics **70**, 61 (2016).
[42] Y.-C. Wang and C.-Y. Wu, Thin Solid Films **561**, 114 (2014).
[43] K. H. Kang, I. Sa, J. C. Lee, E. Fleury, and B. J. Lee, Scripta Materialia **61**, 801 (2009).
[44] W. Y. Wang, H. Z. Fang, S. L. Shang, H. Zhang, Y. Wang, X. Hui, S. Mathaudhu, and Z. K. Liu, Physica B: Condensed Matter **406**, 3089 (2011).
[45] H. Tian, Y. Wang, L. Liu, X. Li, C. Zhang, J. Zhao, C. Dong, and B. Wen, Journal of Non-Crystalline Solids **358**, 1730 (2012).
[46] X. Hui, R. Gao, G. L. Chen, S. L. Shang, Y. Wang, and Z. K. Liu, Physics Letters A **372**, 3078 (2008).
[47] W.-Y. Ching and P. Rulis, *Electronic Structure Methods for Complex Materials: The orthogonalized linear combination of atomic orbitals* (Oxford University Press, 2012).
[48] G. Kresse and J. Hafner, Physical Review B **47**, 558 (1993).
[49] G. Kresse and J. Furthmüller, Physical Review B **54**, 11169 (1996).
[50] G. Kresse and J. Furthmüller, Computational Materials Science **6**, 15 (1996).
[51] P. E. Blöchl, Physical Review B **50**, 17953 (1994).
[52] J. P. Perdew, Physical Review Letters **55**, 1665 (1985).

[53] M. P. Allen and D. J. Tildesley, *Computer simulation of liquids* (Oxford University Press, New York, 1991), p.^pp. 408.
[54] C. Dharmawardhana, R. Sakidja, S. Aryal, and W. Ching, Journal of Alloys and Compounds **620**, 427 (2015).
[55] C. Dharmawardhana, R. Sakidja, S. Aryal, and W. Ching, APL Materials **1**, 012106 (2013).
[56] H. Yao, L. Ouyang, and W. Y. Ching, Journal of the American Ceramic Society **90**, 3194 (2007).
[57] W. Voigt, *Lehrbuch Der Kristallphysik (mit Ausschluss Der Kristalloptik)* (B.G. Teubner, 1928).
[58] A. Reuss, ZAMM - Journal of Applied Mathematics and Mechanics / Zeitschrift für Angewandte Mathematik und Mechanik **9**, 49 (1929).
[59] R. Hill, Proc. Phys. Soc. A **65** (1952).
[60] W. Ching, Journal of the American Ceramic Society **73**, 3135 (1990).
[61] R. S. Mulliken, The Journal of chemical physics **23**, 1833 (1955).
[62] Y. Mo, P. Rulis, and W. Y. Ching, Physical Review B **86**, 165122 (2012).
[63] C. C. Dharmawardhana, A. Misra, S. Aryal, P. Rulis, and W. Y. Ching, Cement and Concrete Research **52**, 123 (2013).
[64] N. Li, R. Sakidja, S. Aryal, and W.-Y. Ching, Physical Chemistry Chemical Physics **16**, 1500 (2014).
[65] S. Aryal, R. Sakidja, M. W. Barsoum, and W.-Y. Ching, physica status solidi (b) **251**, 1480 (2014).
[66] L. Poudel, P. Rulis, L. Liang, and W. Y. Ching, Physical Review E **90**, 022705 (2014).
[67] C. C. Dharmawardhana, A. Misra, and W. Y. Ching, Scientific reports **4**, 7332 (2014).
[68] H. Niu, X.-Q. Chen, P. Liu, W. Xing, X. Cheng, D. Li, and Y. Li, Scientific Reports **2**, 718 (2012).
[69] C. Dharmawardhana, M. Bakare, A. Misra, and W.-Y. Ching, Journal of the American Ceramic Society **99**, 2120 (2016).
[70] L. Poudel, N. F. Steinmetz, R. H. French, V. A. Parsegian, R. Podgornik, and W.-Y. Ching, Physical Chemistry Chemical Physics (2016).
[71] P. Adhikari, M. Xiong, N. Li, X. Zhao, P. Rulis, and W.-Y. Ching, The Journal of Physical Chemistry C **120**, 15362 (2016).
[72] B. Walker, C. C. Dharmawardhana, N. Dari, P. Rulis, and W.-Y. Ching, Journal of Non-Crystalline Solids **428**, 176 (2015).
[73] Q. Yang, A. Mota, and M. Ortiz, Computational Mechanics **37**, 194 (2006).
[74] M. Jiang, M. Naderi, Y. Wang, M. Peterlechner, X. Liu, F. Zeng, F. Jiang, L. Dai, and G. Wilde, AIP Advances **5**, 127133 (2015).
[75] J. Lewandowski*, W. Wang, and A. Greer, Philosophical Magazine Letters **85**, 77 (2005).
[76] C. Li, S. Kou, Y. Zhao, G. Liu, and Y. Ding, Progress in Natural Science: Materials International **22**, 21 (2012).
[77] Z. Y. Liu, Y. Yang, S. Guo, X. J. Liu, J. Lu, Y. H. Liu, and C. T. Liu, Journal of Alloys and Compounds **509**, 3269 (2011).
[78] J. Zhang, S. Pang, and T. Zhang, Science China Physics, Mechanics and Astronomy **53**, 415 (2010).
[79] M. de Jong *et al.*, Scientific Data **2**, 150009 (2015).

[80] S. F. Pugh, The London, Edinburgh, and Dublin Philosophical Magazine and Journal of Science **45**, 823 (1954).
[81] G. N. Greaves, A. L. Greer, R. S. Lakes, and T. Rouxel, Nat Mater **10**, 823 (2011).
[82] S. Nagel and J. Tauc, Physical Review Letters **35**, 380 (1975).
[83] J. Antonowicz, A. Pietnoczka, G. A. Evangelakis, O. Mathon, I. Kantor, S. Pascarelli, A. Kartouzian, T. Shinmei, and T. Irifune, Physical Review B **93**, 144115 (2016).
[84] M. L. Falk and J. S. Langer, Physical Review E **57**, 7192 (1998).
[85] J. S. Langer, Physical Review E **70**, 041502 (2004).
[86] M. H. Cohen and D. Turnbull, The Journal of Chemical Physics **31**, 1164 (1959).
[87] D. Turnbull and M. H. Cohen, The Journal of Chemical Physics **52**, 3038 (1970).
[88] T. Rouxel and Y. Yokoyama, Journal of Applied Physics **118**, 044901 (2015).

List of Figures

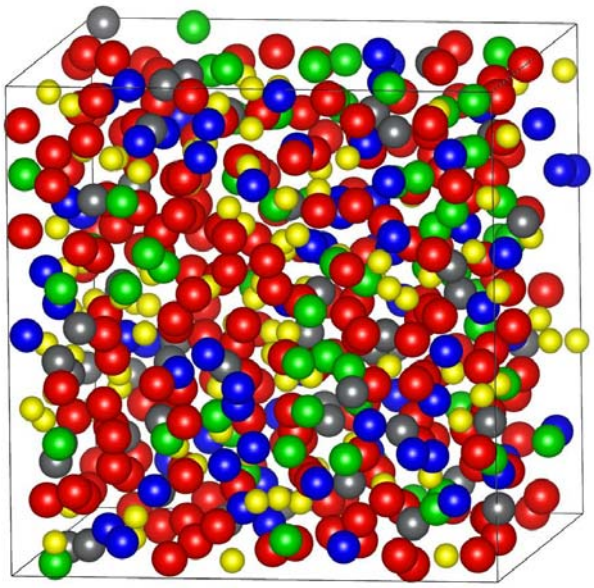

Figure 1. A snapshot of the final configuration obtained by the AIMD calculation for $Zr_{41.2}Ti_{13.8}Cu_{12.5}Ni_{10}Be_{22.5}$ (vit1). There are 211 Zr, 71 Ti, 64 Cu, 51 Ni and 115 Be atoms for a total of 512 atoms. The red, blue, green, yellow and grey circles represent Zr, Ti, Cu, Ni and Be respectively.

(a)

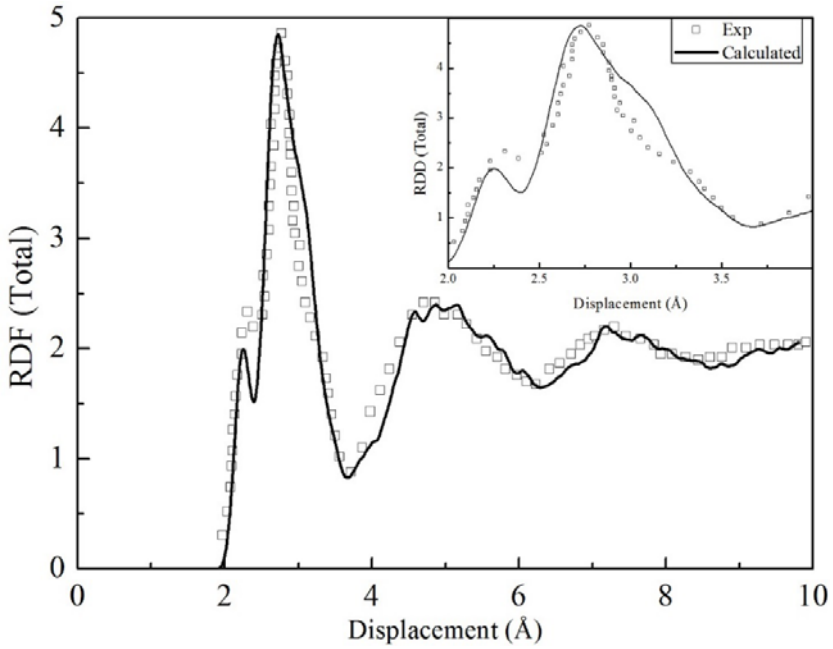

(b)

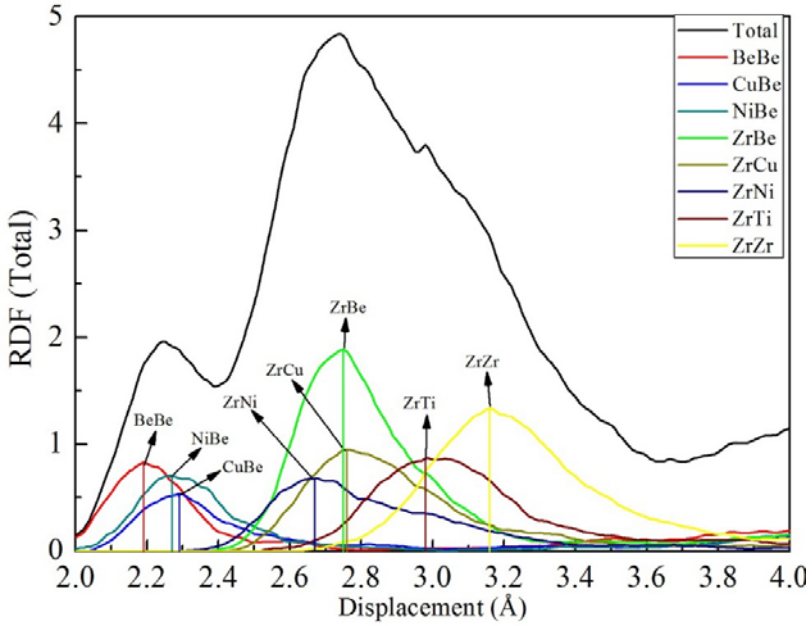

Figure 2. (a) Total Pair Distribution function for $Zr_{41.2}Ti_{13.8}Cu_{12.5}Ni_{10}Be_{22.5}$. (b) Partial Pair Distribution functions for $Zr_{41.2}Ti_{13.8}Cu_{12.5}Ni_{10}Be_{22.5}$.

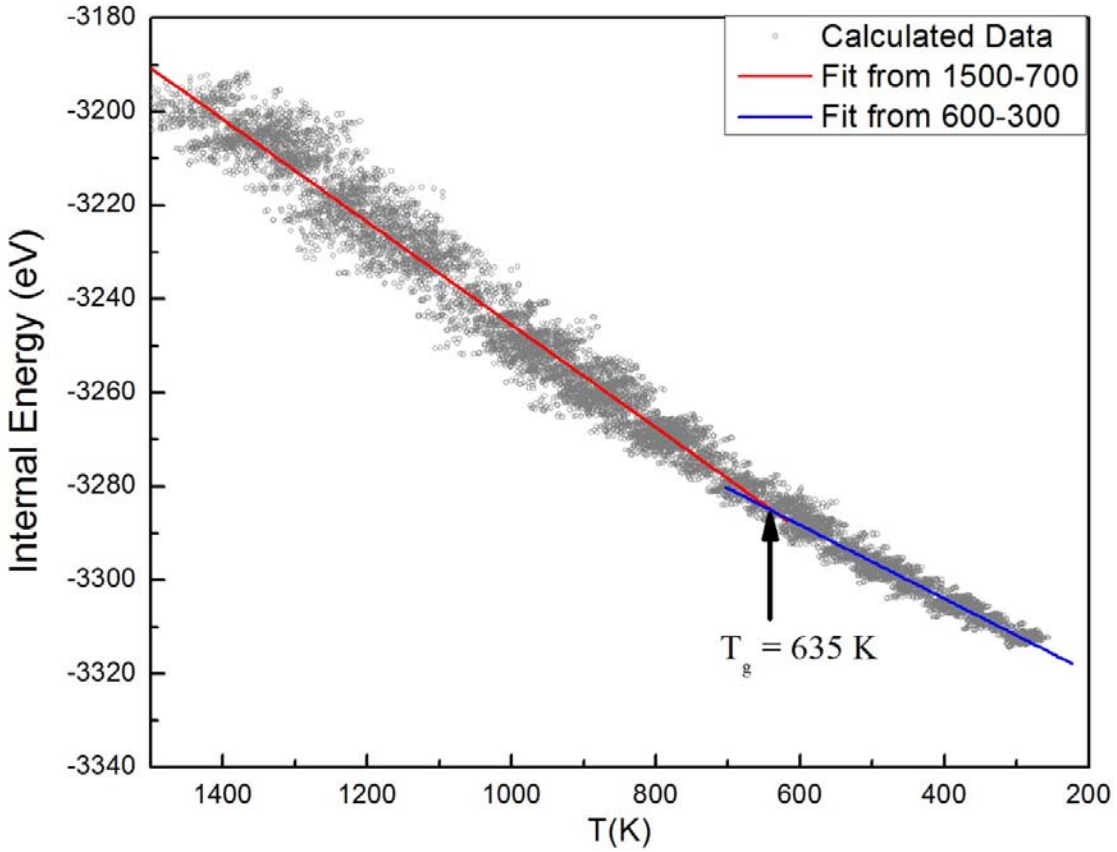

Figure 3. Temperature dependence of the internal energy for vit1 from 1500K to 300 K linearly fitted to straight lines in two temperature ranges. The intersection of the two lines gives the glass transition temperature of 635 K.

(a)

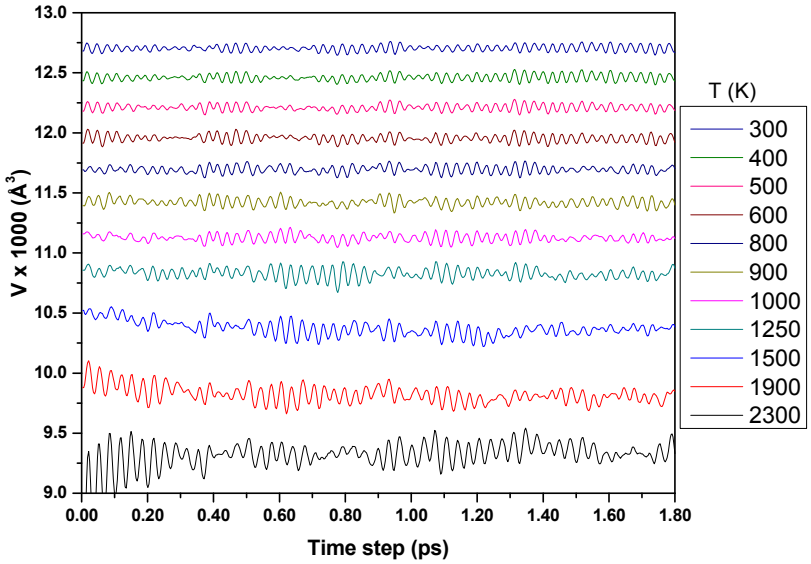

(b)

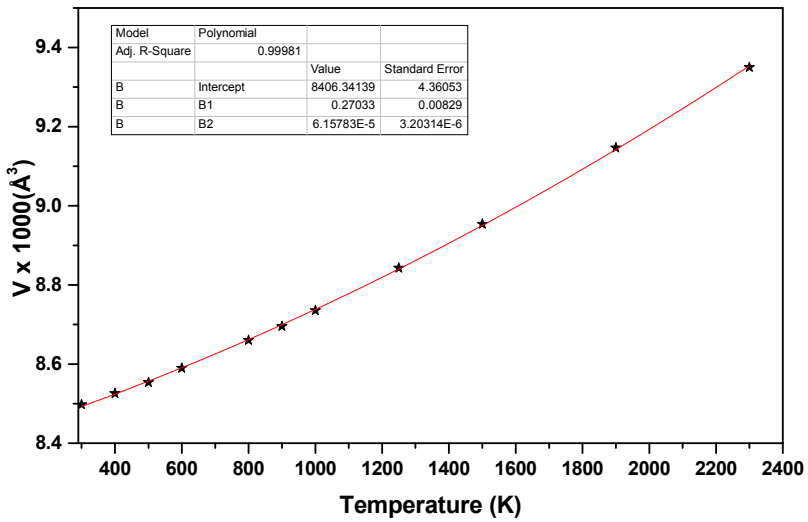

Figure 4. (a) The fluctuation of cell volume at each temperature from the melt to room temperature vs the simulation time step. (b) Average volume of the cell at each temperature. 2nd order polynomial fit is shown in red. The y-axis is in the unit of 10^{-3}(Å).

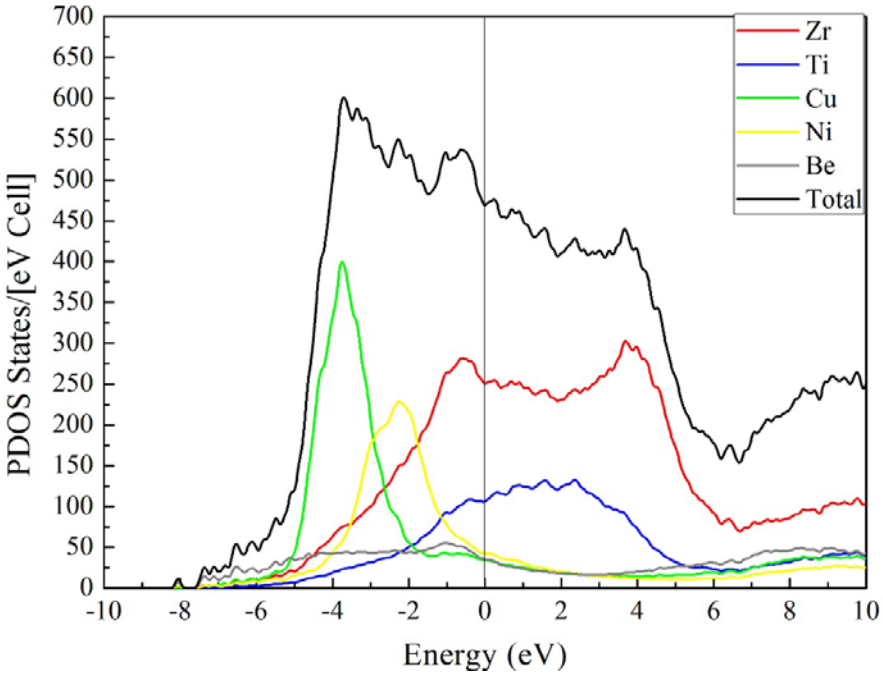

Figure 5. Calculated DOS and PDOS of Zr, Ti, Cu, Ni and Be for vit1. The vertical line depicts the Fermi level.

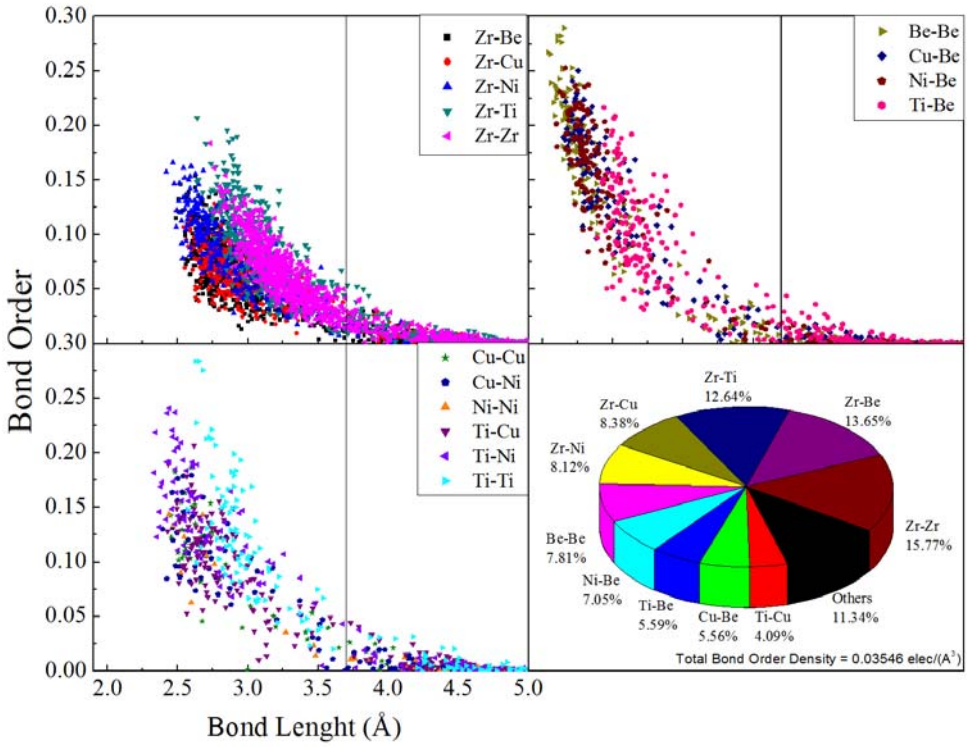

Figure 6. Bond Order vs. Bond Length in (vit1) (a) Zr-related pairs; (b) Be-related pairs, (c) other 6 pairs as indicated. (d) Pie chart for the percentages of the PBOD from different pairs.
The vertical line indicates the position of the sharp minimum of 3.7 Å in the experimental RDF of Fig, 2.

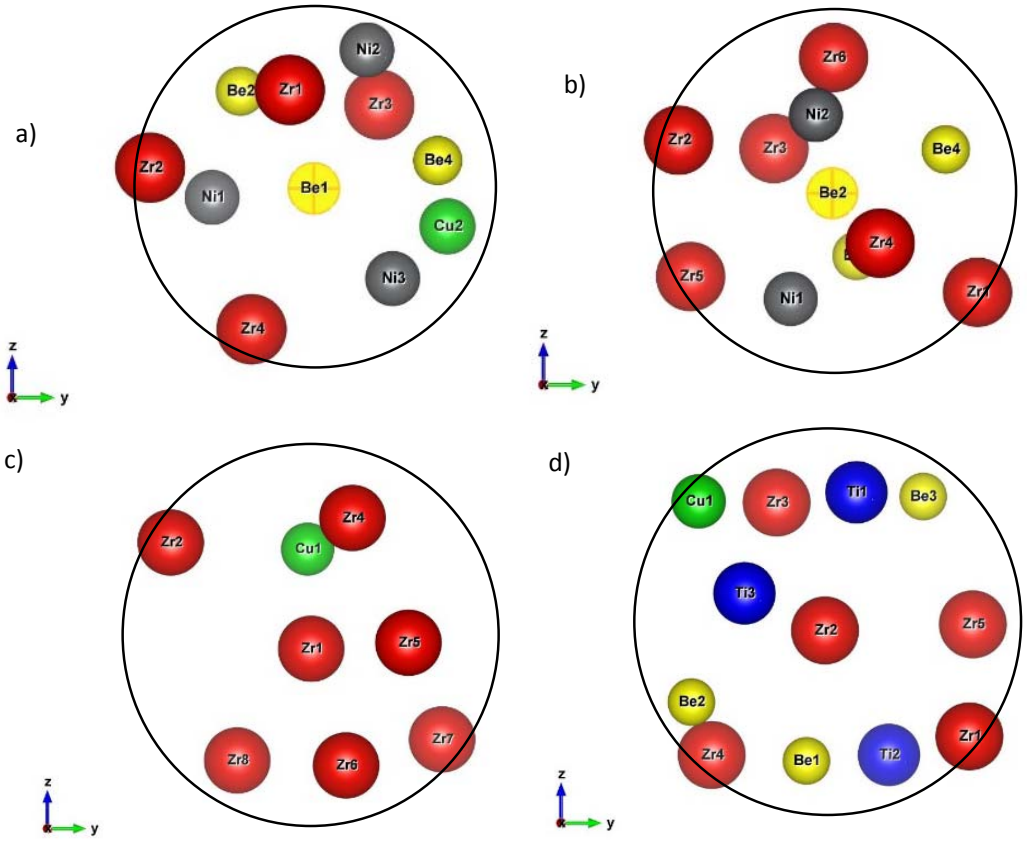

Figure 7. Snapshots of 4 sketches of atomic positions radially in Vireloy model: (a) Be centered (with largest Be-Be BO), (b) Be centered (with smaller Be-Be BO), The Be atoms chosen are the ones with Be-Be BL is at 2.18 Å. (c) Zr centered (with largest Zr-Zr BO), (b) Zr centered (with smaller Zr-Zr BO). The Zr atoms chosen are the ones with Zr-Zr BL is at 3.07 Å. The figure displays all other atoms within the radius equal to the respective BL in the 2 dimensional box with the same size and with color as shown in Fig. 1.

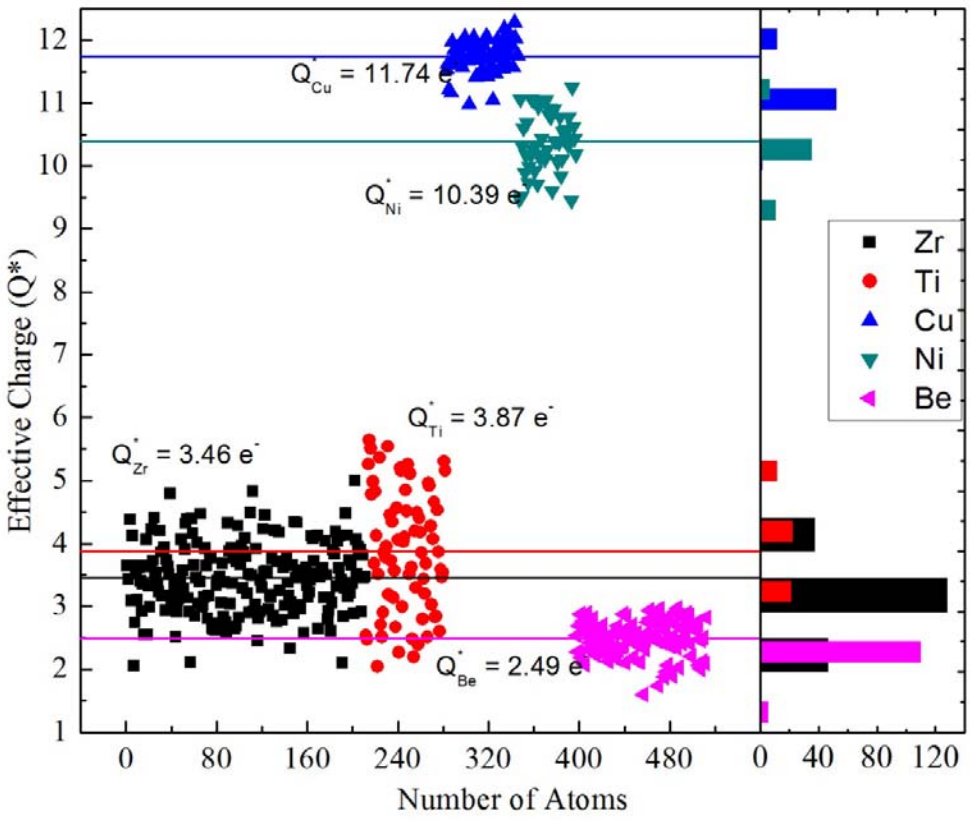

Figure 8. Effective Charges for different types of atoms vs. Atom Number in vit1. The right panel shows histogram plot of distributions of Q* in vit1.